ACS APPLIED MATERIALS & INTERFACES

Research Article

www.acsami.org

3D Artificial Bones for Bone Repair Prepared by Computed Tomography-Guided Fused Deposition Modeling for Bone Repair

Ning Xu,[†,‡] Xiaojian Ye,[†,‡] Daixu Wei,[§] Jian Zhong,*[,§] Yuyun Chen,[§] Guohua Xu,*[,‡] and Dannong He[§]

[‡]Department of Orthopedic Surgery, Changzheng Hospital, Second Military Medical University, Shanghai 200003, People's Republic of China

[§]National Engineering Research Center for Nanotechnology, Shanghai 200241, People's Republic of China

ABSTRACT: The medical community has expressed significant interest in the development of new types of artificial bones that mimic natural bones. In this study, computed tomography (CT)-guided fused deposition modeling (FDM) was employed to fabricate polycaprolactone (PCL)/hydroxyapatite (HA) and PCL 3D artificial bones to mimic natural goat femurs. The in vitro mechanical properties, in vitro cell biocompatibility, and in vivo performance of the artificial bones in a long load-bearing goat femur bone segmental defect model were studied. All of the results indicate that CT-guided FDM is a simple, convenient, relatively low-cost method that is suitable for fabricating natural bonelike artificial bones. Moreover, PCL/HA 3D artificial bones prepared by CT-guided FDM have more close mechanics to natural bone, good in vitro cell biocompatibility, biodegradation ability, and appropriate in vivo new bone formation ability. Therefore, PCL/HA 3D artificial bones could be potentially be of use in the treatment of patients with clinical bone defects.

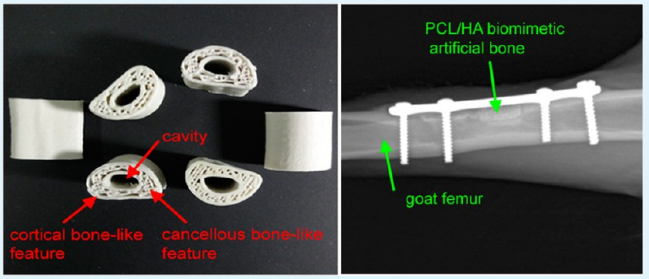

KEYWORDS: *bone segmental defect repair, hydroxyapatite composite, in vivo test, polycaprolactone, computed tomography guided fused deposition modeling*

1. INTRODUCTION

Bone defect repair is a major challenge in orthopedics, dentistry, and cranio-facial surgery, particularly in load-bearing defects.[1−3] Load-bearing bone defects can cause chronic pain, decreased mobility, depression, sleep loss, and significant limitation in quotidian activities. Therefore, the treatment for regeneration of load-bearing bone defects is important for improving the quality of life and prolonging the life of the patient.

To repair the load-bearing bone defects, two types of materials are primarily used in clinical treatments. (1) Autologous bones that are explanted from a different site on the patient (often the iliac crest) can be used.[4,5] They are very effective. However, limited autologous bone availability, the need for additional surgery, the formation of donor site bone defects, possible blood loss and infection, donor site pain, and impracticability of utilizing autologous bone in the osteoporosis patients have restricted their wide application. (2) Commercial artificial bones that primarily consist of inorganic materials can also be used. Some examples include BAM artificial bones (synthetic compound of calcium sulfate salts), and Rebone Gutai artificial bones (calcium phosphate cement), Atlantik artificial bones (hydroxyapatite/ß-tricalcium phosphate), and Pro-dense artificial bones (calcium sulfate/calcium phosphate). Commercial artificial bones are granular or blocky. They have several disadvantages such as their poor biomechanical strength and elastic modulus, low shaping ability, and excessive osteoconduction that could induce a functional loss of repairing bone. Furthermore, these artificial bones are uniform products that cannot meet personalized bone repair needs or accurately match natural bones, which contain both cortical and cancellous regions. Therefore, commercial artificial bones cannot be used for load-bearing bone (femur, tibia, etc.) defect repair. Because of the limitations of these clinically available materials, treatment efficiency has not been fully realized. Approximately 10% of the 13 million yearly fractures in the U.S. that failed to repair.[6,7] The situations in the developing countries are worse because of their poorer medical conditions. Therefore, the medical community has expressed significant interest in the development of new artificial bones that better mimic natural bones for bone repair.

In terms of chemical compositions, natural bone is an inorganic/organic composite that primarily consists of nanostructured hydroxyapatite and collagen fibers.[8] Natural bone structure is generally composed of cortical bone and cancellous bone. Materials scientists have developed biodegradable inorganic materials (hydroxyapatite,[9] β-tricalcium phosphate,[10] etc.) and biodegradable inorganic materials combined with biodegradable polymer (collagen,[11] polycaprolactone,[12] chitosan,[13] etc.) for use in bone repair. Materials scientists have also

Received: May 4, 2014
Accepted: August 18, 2014
Published: August 18, 2014

explored composite scaffolds consisting of polycaprolactone and β-tricalcium phosphate combined with bone morphogenetic protein,[14] which made the scaffolds osteoinductive. However, to the best of our knowledge, until now, artificial bones that mimic both the chemical composition (inorganic/organic materials) and the structure (cortical bone/cancellous bone) of natural bones have not been developed. Even artificial bones with cortical bonelike features and cancellous bonelike feature have also not been developed until now.

Fused deposition modeling (FDM) is a rapid prototyping technique that can produce desired 3D architectures using a computer-aided design model.[15,16] During the fabrication process, thermoplastic materials in the melting chamber are extruded through a heated metal nozzle. The nozzle can be moved both horizontally and vertically and is controlled by computer aided manufacturing software. The extruded materials are deposited onto a receiving station and form a custom-designed architecture. FDM has previously been used to manufacture tissue engineering scaffolds.[17,18] The model for FDM may be generated with modeling software or from medical images such as those obtained by computed tomography (CT).[19,20] CT-guided FDM has been explored to fabricate artificial porous polyurethane human ear scaffolds[21] and artificial porous polybutylene terephthalate canine cancellous bone scaffolds.[22] CT-guided FDM provides a possible method for fabricating artificial bones that mimic both the chemical composition (inorganic/organic materials) and the structure (cortical bone/cancellous bone) of natural bones.

Here, we utilized CT-guided FDM to fabricate polycaprolactone (PCL)/hydroxyapatite (HA) and PCL 3D artificial bones to mimic natural goat femurs. Then, we investigated the in vitro properties of the 3D artificial bones and their in vivo performance in a goat femur bone segmental defect model. The work presented here provides the first example of artificial bones with cortical and cancellous bonelike features. The results indicate that CT-guided FDM is a simple, convenient, relatively low-cost fabrication method that is suitable for the fabrication of natural bonelike artificial bones. The results from these studies also suggest that PCL/HA 3D artificial bones could potentially be used for the treatment of clinical bone defects.

2. MATERIALS AND METHODS

2.1. Synthesis and Characterization of Nanohydroxyapatite. HA nanoscrystals were synthesized by wet synthesis using $(NH_4)_2HPO_4$ and $CaCl_2$ as P and Ca precursors, respectively.[23] Briefly, 120 mL of 0.5 mol/L $(NH_4)_2HPO_4$ aqueous solution was added dropwise into a $CaCl_2$ aqueous/ethanol solution containing 11.10 g of $CaCl_2$ (1:2:8 molar ratio of $CaCl_2$:CH_3CH_2OH:H_2O) at 75 °C. The reaction solution was stirred and the pH was maintained at approximately 10 by adding ammonium hydroxide. White precipitates appeared and increased during the reaction process. Then, the suspension was continuously stirred at 75 °C for 3 h and aged at room temperature for 24 h. The precipitates were washed by ten cycles of centrifugation and water-washing (5 min centrifugation at 5000 rpm, and redispersion in Milli-Q water). The washed precipitates were frozen at −80 °C for 24 h. Finally, the precipitates were freeze-dried for 24 h and white n-HA powder was obtained. Transmission electron microscopy (TEM) of the n-HA composites was performed with a JEM2100 transmission electron microscope (JEOL, Tokyo,Japan) operated at an accelerating voltage of 200 kV. The ATR-FTIR spectrum of the n-HA composites was obtained on a Nicolet 6700 spectrometer (Thermo Fisher Scientific, USA) with an attenuated total reflectance accessory (ATR) at room temperature. X-ray diffraction (XRD) patterns of n-HA were recorded by a D/MAX-2200PC X-ray diffractometer (Rigaku, Tokyo, Japan) using CuKa radiation. The sample was scanned from 20° to 60° with a scanning rate of 4°·min^{-1}.

2.2. Fabrication of PCL/HA or PCL 3D Artificial Bone. A normal goat leg was scanned by X-ray CT (μCT-20, Scanco Medical AG, Switzerland) at medium resolution (600 X-ray projections with 512 × 512 pixels bitmap image, 18 μm resolutions). A generator rating of 53.2 kW enabled a current of 139 mA•s at 120 kV. The resulting CT data (Figure 2A) were transformed into a 3D model (Figure 2B) by CT reconstruction. Then, the 3D model was imported into Mimics software (ver.9.1, USA). The images were segmented by first altering the contrast and then selecting a suitable threshold value to isolate the bony structure (Figure 2C). The typical long (1.5 cm) load-bearing femur bone model (Figure 2D) was selected and exported in STL format, which is the standard format used by FDM machines.

The STL-formatted file was imported into the FDM software and revised to obtain a bone model that mimics cortical and cancellous structure of natural bone (Figure 2E). Melt blending of PCL with HA at a mass ratio of 7:3 was carried out at 100 °C and 100 rpm for 10 min using a twin counter-rotating internal mixer connected to a control unit (Rheomix 600 and Rheocord 9000, respectively, Haake, Germany). PCL/HA and PCL were used to fabricate 3D artificial bones by fused deposition modeling.

2.3. Porosity Measurements. The 3D artificial bone porosity was measured with a liquid displacement technique. Ethanol was used as the substitution liquid because it penetrated easily into the pores of the 3D artificial bones but not into the bulk. Briefly, the cancellous bonelike features of the 3D artificial bone were sealed with adhesive tapes, and the bone was immersed in a graduated cylinder containing 10 mL of ethanol for 1 min. The adhesive tapes made sure no ethanol enter the pores of the 3D artificial bones. The total volume in the graduated cylinder was recorded as V_1 mL. Then, the artificial bone was taken out, the adhesive tape was removed, and the bone was dried. Afterward, the 3D artificial bone was immersed in a graduated cylinder with 10 mL of ethanol for 5 min to allow the ethanol to penetrate into the pores. The total remaining volume was then recorded as V_2 mL. Porosity was calculated by the following equation

$$\text{porosity}\ (\%) = (V_1 - V_2)/(V_1 - 10) \times 100\% \quad (1)$$

Six specimens were measured for each sample.

2.4. Compression Measurements. Natural goat femur bones were obtained from normal goat legs. Compression measurements of the artificial and natural bones with lengths of 1.5 cm were performed along the longitudinal axis of the bones with a universal testing machine (Shimazu AG-2000A) using displacement control (4 mm/min) at ambient conditions.[24] The load−displacement curves were recorded continueously until failure. Six specimens were measured for each sample. The compressive strength was calculated according to the following equations[25]

$$\text{compressive strength} = F/S \quad (2)$$

where F and S are the maximal load value and the cross-sectional surface area of the untreated sample, respectively. The cross sectional surface area of the BAM artificial bone was calculated by multiplying its width and height. The cross sectional surface areas of the PCL/HA, PCL artificial bones and natural goat femur bones were calculated with a digital pixel counting method. Briefly, the sample was placed onto a black desk with a ruler, and the cross sectional surfaces were captured with a digital camera. Then, the pictures were opened in Photoshop, and the digital pixel numbers of the cross-sectional surface areas and a 1 cm^2 black area were determined by using the select/color range window. Finally, the cross-sectional surface area was calculated by the following equation:

$$\text{cross-sectional surface area} = D_c/D_b\ (\text{cm}^2) \quad (3)$$

where D_c and D_b are the numbers of digital pixels in the sample cross sectional surface and in the 1 cm^2 black area, respectively.

The elastic modulus was calculated as the initial slope (elastic regime) of the stress−strain curves for each sample.[26]

2.5. In Vitro Cell Biocompatibility Measurements. Mouse osteoblast-like cells (MC3T3-E1, purchased from the Cell Bank of Chinese Academy of Sciences, Shanghai, China) were used to investigate the cell proliferation on the PCL/HA scaffolds, PCL scaffolds, and BAM artificial bones. The cells were cultured in DMEM (Gibco, USA) with 10% fetal bovine serum (FBS, Gibco, USA) in an incubator with 5% CO_2 at 37 °C.

PCL/HA scaffolds and PCL scaffolds were placed into 24-well tissue culture plates (TCPs), sterilized by immersion in 75% (v/v) ethanol for 6 h, and washed three times with 10 mM phosphate buffered saline (PBS) to remove ethanol. Then, the scaffolds were immersed in DMEM with 10% FBS for 2 h, and 100 000 MC3T3-E1 cells were seeded onto each scaffold. The scaffolds were transferred to new 24-well TCPs after 1 day of incubation. At the designated time points (1, 4, and 7 days), cell distributions, viabilities, and morphologies were assessed.

The MC3T3-E1 cell distributions were observed by laser scanning confocal microscopy (LSCM). The live cells were fixed in 4% paraformaldehyde for 20 min at room temperature and washed 3 times with 10 mM PBS. Then, the cells were permeabilized with 0.5% Triton X-100 for 10 min and washed 3 times with 10 mM PBS. Afterward, the cell actin and nuclei were labeled with 0.6 mL of 5 μg/mL Alexa Fluor 594 phalloidin (Life Tech, USA) and 0.6 mL of 10 μg/mL DAPI (Life Tech, USA), respectively, for 5 min at room temperature. Finally, labeled cells were observed with LSCM (TCS SP5, Leica, Germany). Six specimens were prepared for each sample.

MC3T3-E1 cell viabilities were analyzed with a CCK-8 assays.[27] Briefly, 0.5 mL of DMEM containing 10% CCK-8 (Fanbo Biochemicals, China) were added to each well. After 2 h, 100 μL of the above solution was transferred to a 96-well plate. Solution absorbances were measured at 450 nm with a microplate reader (Infinite F50, TECAN, Switzerland). The absorbance values were corrected by subtracting the signal of a mixture of 90 μL DMEM and 10 μL CCK-8. BAM artificial bones were used as controls. Six specimens were prepared for each sample.

MC3T3-E1 cell morphologies were observed by SEM. First, adhered cells were immobilized with 5% glutaraldehyde for 30 min and washed with PBS. Then, the fixed cells were successively immersed in a series of ethanol solutions (50, 70, 80, 90, 95, and 100%) for 10 min. Finally, the cells were observed with SEM (Hitachi S-4800, Japan) at an accelerated voltage of 10 kV. Three specimens were prepared for each sample.

2.6. Segmental Load-Bearing Bone Defect Model. Thirty adult goats weighing 20−30 kg (obtained from the Laboratory Animal Center, Shanghai Jiao Tong University) were randomly divided into 5 groups. The use of goats and the experimental protocols were approved by the Institutional Animal Care and Use Committee of Shanghai Jiao Tong University. The goats were anaesthetized and a partial goat femur bone segmental defect model was constructed. Briefly, the wool on the goat legs was shaved (Figure 5A), and the goat legs were disinfected with tincture of iodine (Figure 5B). The femoral shaft was exposed with a 6 cm longitudinal incision made using a standard lateral approach to the femur (Figure 5C). Then, a bone segment of 1.5 cm in length and approximately half of the femoral shaft in depth was excised from the mid diaphyseal region using a Gigli saw and an electrical drill to construct a partial long load-bearing femur segmental bone defect model (Figure 5D). The periosteum was also partially removed during this process.

2.7. Artificial Bone Implantation. The upper portions of the PCL/HA artificial bones were cut and used as implants. The size of the upper portion of the artificial bones was dependent upon the size of the goat segmental bone defect. The defects were left untreated/empty (control) or were reconstructed with PCL/HA 3D artificial bones (Figure 5E), PCL 3D artificial bones (Figure 5E), BAM artificial bones (Figure 5F), or autologous bones that were originally excised from the mid diaphyseal region (Figure 5G). Then, titanium nails with four distal locking holes and four screws were used for implant immobilization (Figure 5H). Finally, the 6 cm longitudinal incision was sutured (Figure 5I). The six goats in each experimental group were randomly divided into two observation period groups: 4 and 12 weeks postimplantation.

2.8. X-ray Observation. Soft X-ray observation was taken at 4 and 12 weeks postimplantation by a Siemens Luminos Select X-ray in standard projection on the operated limb at 43 kV and 2 mA for 1.5 s.

2.9. Histological Observation. The goats were sacrificed at 4 and 12 weeks postimplantation for histological observation. The femurs were harvested from the goat legs (the soft tissues were removed from the bone). Then, the titanium nails with four distal locking holes were removed. The artificial bones and the surrounding host bone tissues were excised and fixed in a 4% paraformaldehyde solution at 4 °C for 24 h. After washing with water, fixed specimens were dehydrated by immersion in graded ethanol solutions (70, 75, 80, 85, 90, 95, and 100%) for 24 h in each solution. After dehydration, specimens were embedded in the medium of poly(methyl methacrylate) (methyl methacrylate, Merck, Germany) and sectioned with a microtome (Leica, SP1600, Leica SP1600) equipped with sturdy tungsten carbide knives. The sections were polished and stained with picric acid magenta to label collagen. Then, the sections were imaged with a digital camera and an optical microscope (Leica, DMI 4000B, Germany).

2.10. Statistical Analysis. All data are presented as the mean value ± standard deviation (SD). Statistical comparisons were performed using one-way ANOVA, and $p < 0.05$ was considered to be significant.

3. RESULTS

3.1. Synthesis and Characterization of Nanohydroxyapatite. As described in our previous work,[23] the HA nanocrystals were synthesized by wet chemical method using $(NH_4)_2HPO_4$ and $CaCl_2$ as P and Ca precursors, respectively. Then, the synthesized HA nanocrystals were characterized. TEM (Figure 1A) demonstrated that HA nanocrystals were typically 40−150 nm in length and 20−30 nm in diameter. The ATR-FTIR spectrum (Figure 1B) displays a broad peak at 3420 cm^{-1} that corresponds to OH^- and sharp peaks at 1033 and 957 cm^{-1} that correspond to PO_4^{3-}. In the XRD spectrum (Figure 1C), all of the diffraction peaks were well-assigned to poor crystalline HA and no peaks from other calcium

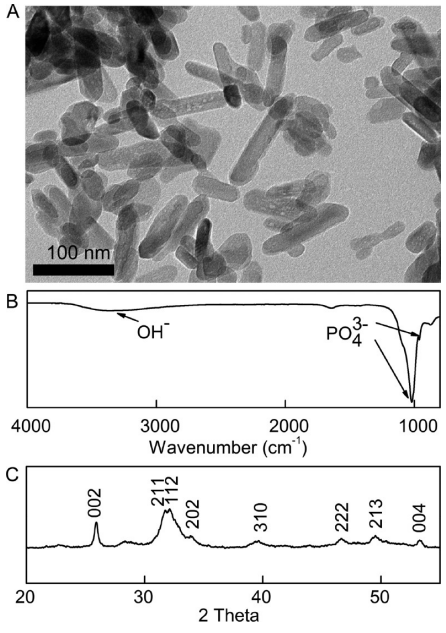

Figure 1. Characterization of synthesized hydroxyapatite nanoscrystals. (A) TE micrograph, (B) ATR-FTIR spectrum, (C) XRD spectrum.

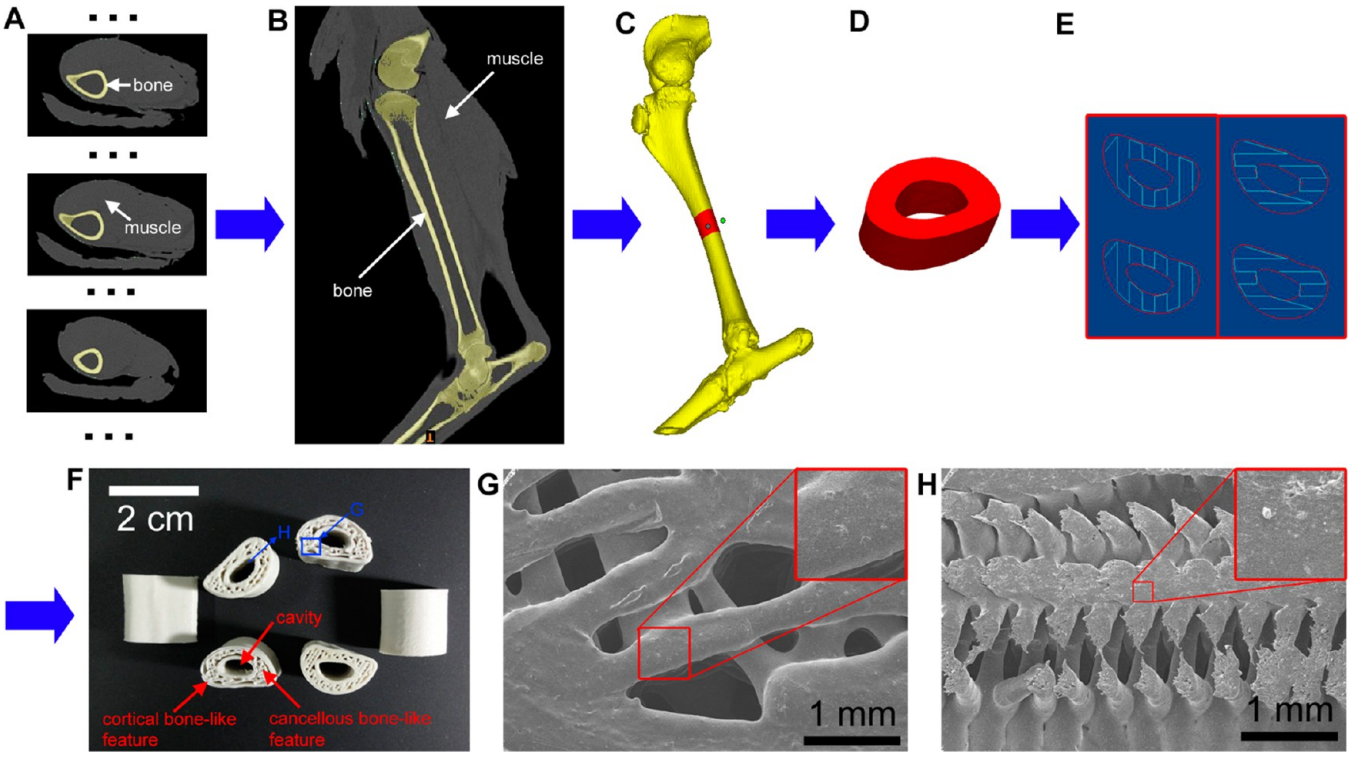

Figure 2. Fabrication and characterization of 3D artificial bones. (A) CT data of normal goat leg. (B) Sectional image of 3D model of normal goat leg by CT reconstruction from A. (C) Sectional image of 3D bony structure of goat femur. (D) Typical long (1.5 cm) load-bearing femur bone model. (E) Left and right images show the designed alternate slices used to fabricate 3D artificial bones. (F) The prepared PCL/HA 3D artificial bones. (G) SEM image of PCL/HA 3D artificial bone surface.The upper-right image is magnified from the corresponding area. (H) SEM image of cross-section of PCL/HA 3D artificial bones. The upper-right image is magnified from the corresponding area.

phosphate phases were detected. All of these analyses demonstrated that HA nanocrystals were successfully synthesized in our work.

3.2. Fabrication and Characterization of PCL/HA and PCL 3D Artificial Bones by CT-Guided FDM. Using CT-guided FDM, PCL/HA and PCL 3D artificial bones were fabricated (Figure 2A–F). The fabricated 3D artificial bones (Figure 2F) had structures similar to natural goat femurs. Cross-sectional scanning electron micrographs (Figure 2G, H) of PCL/HA artificial bones displayed the cancellous bonelike features. Some particle-like features were observed on the artificial bone surfaces (Figure 2G) and in the artificial bone bulks (Figure 2H), which indicated that HA nanocrystals were present in the PCL/HA 3D artificial bone. Based on SEM observations, the PCL/HA 3D artificial bone had interconnected pores with a diameter of 765 ± 83 μm and strands with a thickness 280 ± 33 μm. The PCL 3D artificial bone had interconnected pores with a diameter of 746 ± 71 μm and strands with a thickness 275 ± 28 μm. These sizes were similar to previously prepared porous scaffolds.[28,29]

3.3. Porosity Measurements. Using a liquid displacement technique, 3D artificial bone porosity was measured. The porosities of PCL/HA and PCL 3D artificial bones were 26 ± 8% and 23 ± 6%, respectively. These porosities were lower than those of previously prepared porous scaffolds,[28,29] which could be attributed to the presence of cortical bonelike features in the current scaffolds.

3.4. Compression Measurements of Artificial Bones and Natural Bone. Compression measurements were performed to compare the artificial bone mechanics to those of natural bones. Figure 3 displays the force–displacement

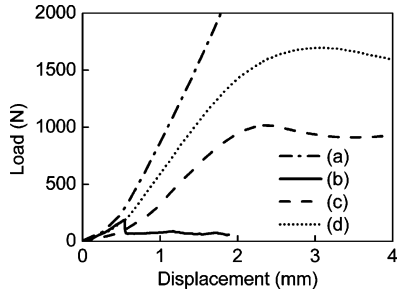

Figure 3. Typical force–displacement curves of artificial and natural bones. (a) Adult goat femur, (b) BAM artificial bone, (c) PCL 3D artificial bone, and (d) PCL/HA 3D artificial bone.

curves of artificial and natural bones. The compressive strength and elastic modulus were calculated from these curves, as shown in Table 1. The orders of maximum load, compressive strength, and elastic modulus of the artificial and natural bones were: adult goat femur > PCL/HA 3D artificial bone > PCL 3D artificial bone > BAM artificial bone. Compared with the compressive strength (38.7 ± 0.3 MPa) and elastic modulus (297.8 ± 7.1 MPa) of bulk PCL,[30] PCL 3D artificial bones had reduced compressive properties, which may be due to the cancellous bonelike features in the artificial bones, as shown in Figure 2F. Compared with the PCL 3D artificial bone, the PCL/HA 3D artificial bone had a higher compressive strength and elastic modulus, which may be due to the addition of nano HA.[31]

3.5. In Vitro Cell Biocompatibility Studies. Porous scaffolds with interconnected networks are a promising material for tissue engineering and regeneration because they can guide

Table 1. Compressive Strength and Elastic Modulus of Artificial and Natural Bones

materials	compressive strength (MPa)	elastic modulus (MPa)
PCL/HA 3D artificial bone	15.43 ± 1.28	80.16 ± 3.18
PCL 3D artificial bone	9.09 ± 0.74	62.7 ± 2.3
BAM artificial bone	2.49 ± 0.48	32.03 ± 8.45
adult goat femur	>18.17 ± 2.23[a]	>132.22 ± 15.66[a]
natural cortical bone[63]	131−224	17×10^3 to 20×10^3
natural cancellous bone[63,64]	5−10	50−100
bulk PCL[30]	38.7 ± 0.3	297.8 ± 7.1

[a]2 kN force transducer was used in the compression measurements.

cell attachment and growth/ingrowth.[28] Therefore, the cancellous bonelike features of the PCL/HA and PCL 3D artificial bones may serve a more important role in new bone formation than the cortical bonelike features. Therefore, in this work, in vitro cell biocompatibility of porous PCL/HA scaffolds, porous PCL scaffolds, and BAM artificial bones was assessed. MC3T3-E1 mouse osteoblast-like cell distributions, viabilities, and morphologies in response to different artificial bone biomaterials were studied, as shown in Figure 4.

At the designated time points (1, 4, and 7 days), the actin and nuclei of MC3T3-E1 cells grown on the three artificial bone biomaterials were labeled by Alexa Fluor 594 phalloidin and DAPI, respectively. Then, the cell numer and distribution of MC3T3-E1 cells were observed using LSCM (Figure 4A). In the first 24 h of culture, few MC3T3-E1 cells adhered to the

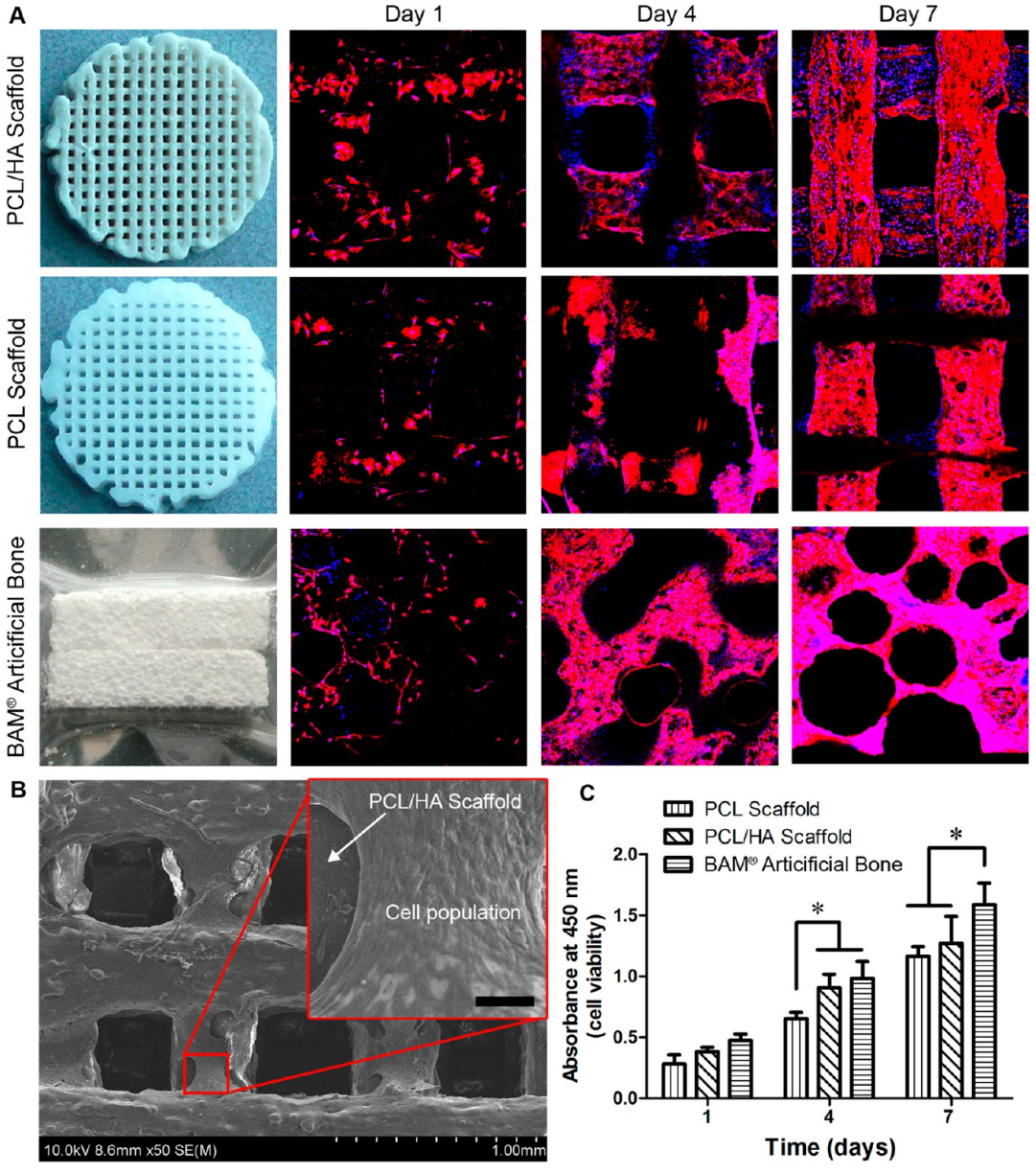

Figure 4. In vitro cell biocompatibility studies of PCL/HA scaffold, PCL scaffold, and BAM artificial bone. (A) LSC micrographs of MC3T3-E1 cell distributions on PCL/HA scaffold, PCL scaffold, and BAM artificial bone, from top to bottom, respectively. (B) SE micrographs of MC3T3-E1 cell morphologies on PCL/HA scaffold. (C) CCK-8 assay for MC3T3-E1 cell proliferation on PCL/HA scaffold, PCL scaffold, and BAM artificial bone. *$P < 0.05$, $n = 6$.

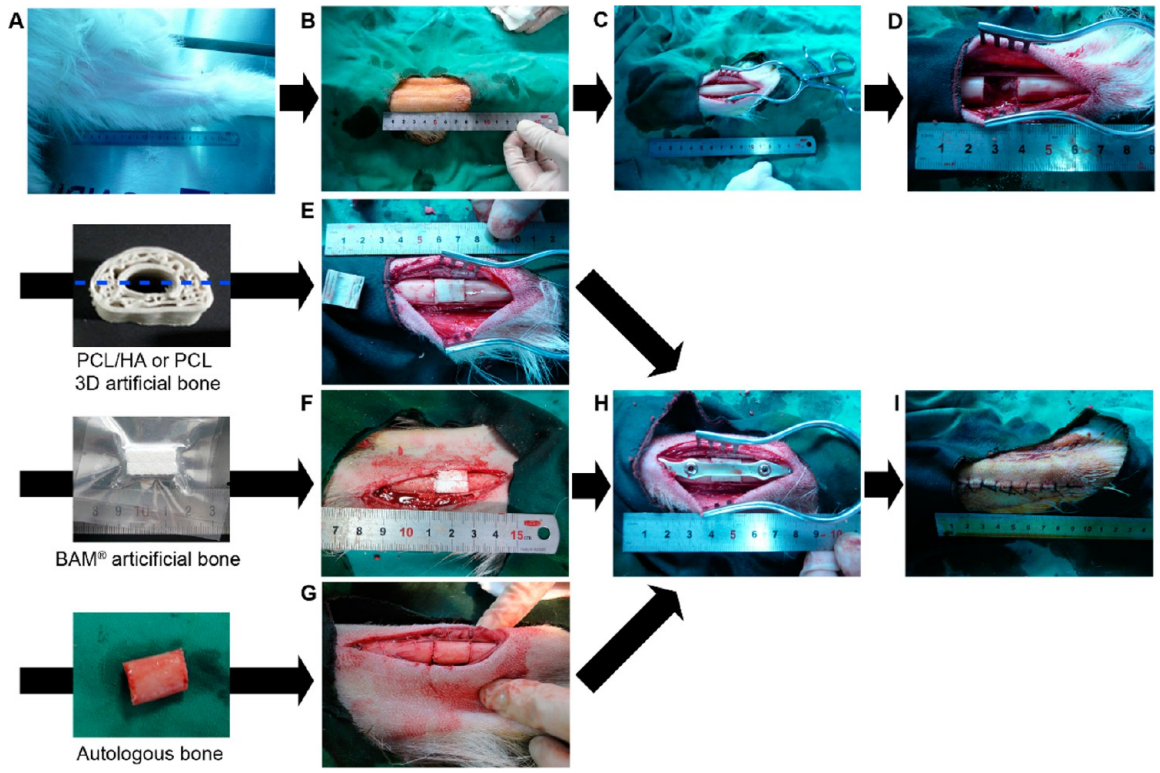

Figure 5. Construction of segmental load-bearing bone defect model and artificial bone implantation. (A) Goat leg after shaving. (B) Goat leg after disinfection with tincture of iodine. (C) Femoral shaft exposed through a 6 cm longitudinal incision. (D) Load-bearing bone segmental defect model. A bone segment of 1.5 cm in length and half of the femoral shaft in depth was excised from the mid-diaphyseal region. (E) Upper portions of PCL/HA and PCL 3D artificial bones (the upper part of the blue dashed line) was cut and implanted in the defect site and the other half was shown in the left side of this image. (F) Implanted BAM artificial bone in the defect site. (G) Implanted autologous bone in the defect site. (H) Goat femur immobilization by titanium nails. (I) Sutured goat leg.

surfaces. Then, the number of viable cells grown on the biomaterials increased over time. After 7 days of incubation, cell populations had formed on the surfaces.

Activities of MC3T3-E1 cells grown on different artificial bone biomaterials were studied by a CCK-8 assay after 1, 4, and 7 days of incubation (Figure 4C). As expected, MC3T3-E1 cells grew well on all scaffolds over 7 days. The MC3T3-E1 cell activities on the three scaffolds were similar at day 1 ($p > 0.05$). At day 4, the activities of cells on the BAM artificial bone and PCL/HA scaffold were similar ($p > 0.05$), however, the cell number on these two surfaces were higher than on PCL scaffold ($p < 0.05$). At day 7, BAM artificial bone showed the best cell activity among the three materials ($p < 0.05$), and the activities on the PCL/HA and PCL scaffolds were similar ($p > 0.05$).

The cell morphology of MC3T3-E1 cells on the PCL/HA scaffold at 7 days were observed by SEM. The micrographs (Figure 4B) showed that cells grew to the high densities and cell populations were formed on the scaffolds, similar to the observations from the LSCM results (Figure 4A).

The results above demonstrated that MC3T3-E1 cells proliferated well on the three artificial bone biomaterials, indicating their in vitro cell biocompatibility. The relative in vitro cell proliferation abilities on the three samples were as follows: BAM artificial bone > PCL/HA scaffold > PCL scaffold.

3.6. Segmental Bone Defect Model Construction and Artificial Bones Implantation. In clinics, complete segmental bone defects are less common relative to partial segmental bone defects. Complete segmental bone defects make femur fixation after implantation more difficult and increase the risk of infection, bone fracture, and animal death when compared to partial segmental bone defects. Therefore, a partial segmental bone defect model was employed in this work (Figure 5A–D). Artificial bones and autologous bones were implanted into the bone defect models (Figure 5E-I). The process was facile and took only approximately 20 min. The segmental bone defect model without an implant served as a negative control. During the implantation process and the subsequent 3 months, the goats did not show obvious discomfort.

3.7. X-ray Observation. Figure 6 displays the X-ray images of goat femurs at 4 and 12 weeks postimplantation. The untreated segmental bone defect group (control) did not show obvious bone repair, even after 12 weeks, which demonstrated that appropriate treatments were needed to induce the bone repair. The autologous bone began to fuse with the goat femur at 4 weeks postimplantation and did not show an obvious gap between the implant and the surrounding bones at 12 weeks postimplantation. This result confirmed that autologous bone was the best bone repair option, and it serves as the current gold standard for the research and development of bone repair biomaterials.

At 4 weeks postimplantation, differences were observed in the egdes between the implanted bones and the surrounding femur bones for the five groups. The bone fusion order was as follows: autologous bone > PCL/HA 3D artificial bone > BAM artificial bone > PCL 3D artificial bone > control. These relationships also applied to the bone osteoconduction abilities.

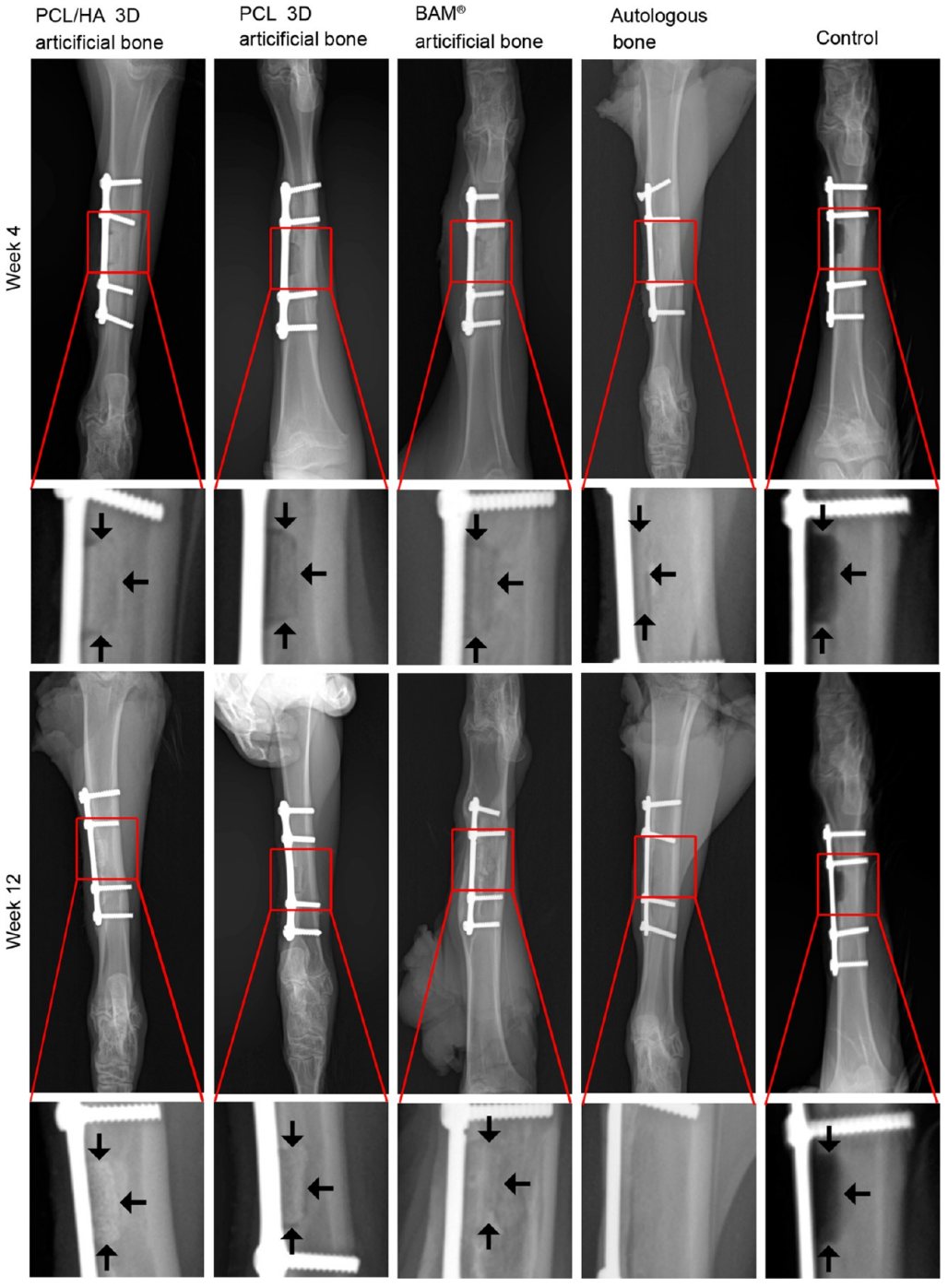

Figure 6. X-ray images of goat legs at 4 and 12 weeks postimplantation.The lower images were magnified from the corresponding regions. Black arrows indicate the bone defect edges.

At 12 weeks postimplantation, obvious differences were observed in the five groups. The BAM artificial bone group had excess callus formation. The PCL 3D artificial bone group had clearly present edges (indicated by black arrows). For the PCL/HA 3D artificial bone group, small gaps between the artificial bones and the defect bones were not observed, and appropriate callus formed. Therefore, between 4 and 12 weeks, the relative in vivo bone osteoconduction of the five groups was as follows: BAM artificial bone > PCL/HA 3D artificial bone > autologous bone > PCL 3D artificial bone > control. Moreover, PCL/HA 3D artificial bones had appropriate bone osteoconduction ability for the treatment of goat femur segmental defects.

The 4 and 12 week observations showed that PCL/HA 3D artificial bone osteoconduction ability was the most similar to that of autologous bone, which implied that PCL/HA 3D artificial bones could potentially be employed to treat long load-bearing goat femur segmental bone defect.

3.8. Histological Observation. Figure 7 displays digital camera images of the histological evaluation of artificial bones in the goat femur environments at 4 and 12 weeks postimplantation. The BAM artificial bone group showed the fastest new bone formation (indicated by green arrows). At 4 weeks postimplantation, the transparent artificial bones (indicated by yellow arrows) degraded (indicated by blue

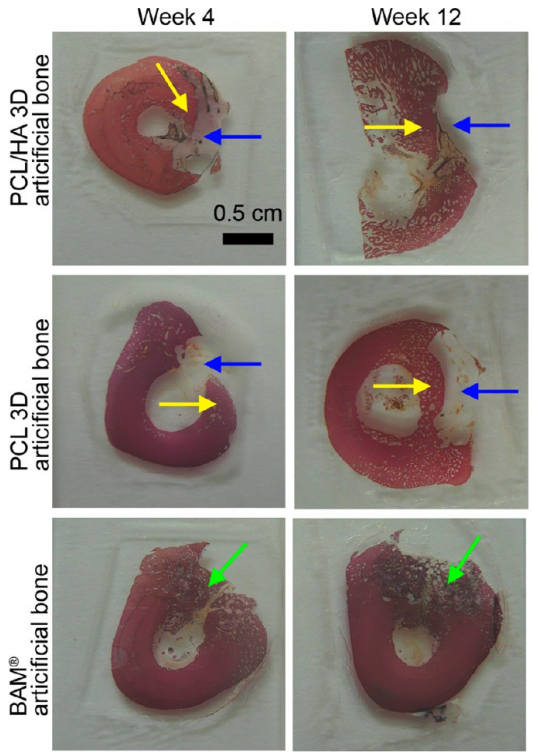

Figure 7. Histological observation of the defect sites at 4 and 12 weeks postimplantation by digital camera. Blue arrows indicate artificial bones. Yellow arrows indicate newly formed bones. Green arrows indicate the mixture between the BAM artificial bone and newly formed bones. The scale bar is 0.5 cm and applies to all images.

arrows) and new bone formed (indicated by blue arrows) in the PCL/HA and PCL 3D artificial bone groups. Over time, the artificial bones continued to degrade (indicated by blue arrows) and new bone continued to form and connect to surrounding bone (indicated by yellow arrows). Therefore, these artificial bones had good in vivo biocompatibility abilities, biodegradation, and osteoconduction. The order of new bone formation speeds with the materials was as follows: BAM artificial bone > PCL/HA 3D artificial bone > PCL 3D artificial bone.

To observe the interfaces between the implant materials and surrounding bones, a histological evaluation of artificial bones in the goat femur environment at 4 and 12 weeks postimplantation was perfomed by optical microscope, as shown in Figure 8. The BAM artificial bone group demonstrated new bone formation (in rose color, indicated by green arrows) and migration into the artificial bone pores (indicated by red arrows) at 4 weeks postimplantation. At 12 weeks postimplantation, almost all of the BAM artificial bone pores were filled with new bone (in rose color, indicated by green arrows).

For the PCL 3D artificial bone group, at 4 weeks postimplantation, a new bone formation zone (between the two dashed green lines in the image) appeared between the transparent PCL artificial bone and the native femur. Several-hundred-micrometer-sized PCL particles (in white color, indicated by blue arrows) appeared among the new bones (in rose color, indicated by green arrows). These PCL particles may have been degradation products from the artificial bone. At 12 weeks postimplantation, the new bone formation zone (below the dashed green line in the image) had expanded, which demonstrated that new bone increased over time. In addition, the number of PCL particles (in white color, indicated by blue arrows) increased over time, which indicating artificial bones degradation over time. Previous work showed PCL broke into low-molecular-weight pieces at the end of 30 months when PCL was implanted under the skin of rats.[32] In this work, PCL began to degrade at 4 weeks postimplantation. The possible reason is that the blood supply in goat femur bone is more abundant than that in rat subcutaneous tissues. Richer blood supply results in faster PCL degradation in goat femur bone model.

For the PCL/HA 3D artificial bone group, at 4 weeks postimplantation, a new bone formation zone (between the two dashed lines in the image) appeared between the artificial bone and the femur. Several-hundred-micrometer-sized PCL particles (in white color, indicated by blue arrows) appeared on the new bone (in rose color, indicated by green arrows). In addition, there was a small number of black particles (indicated by yellow arrows) in the new bone formation zone. Considering that the color was similar to that in the histological image of the BAM artificial bone and that there were black particles in the artificial bone zone, these particles may have been HA pieces those were degraded from the artificial bone. At 12 weeks postimplantation, the new bone formation zone (below the dashed green line in the image) had expanded, which demonstrated that new bone increased over time. In addition, the number of PCL particles (in white color, indicated by blue arrows) and HA particles (in black color, indicated by yellow arrows) increased over time, which demonstrated that the PCL/HA 3D artificial bones degraded over time.

The histological results (Figure 7 and 8) showed the degradation and osteoconduction behaviors of artificial bones in goat femurs and demonstrated that new bone formed and that the artificial bones degraded over time. Histology confirmed that the osteoconduction ability of these artificial bones, and the order of new bone formation speeds with the implant materials was as follows: BAM artificial bone > PCL/HA 3D artificial bone > PCL 3D artificial bone, which is consistent with the X-ray observations (Figure 6). Additionally, the three biomaterials possessed good in vivo biocompatibility, which is consistent with the in vitro cell biocompatibility assay (Figure 4).

4. DISCUSSION

The Freedonia Group's industry study report of "Implantable medical devices to 2014 & 2019" indicated that US demand for implantable medical devices is expected to increase 8.3% annually up to $49 billion in 2014.[33] According to the report, bone implants will be among the fastest growing product categories. The development of next generation implantable medical devices and improved materials based on new technologies such as rapid prototyping are the primary reasons for the expected growth.

Load-bearing bone defect repair has attracted increasing attention from scientists and engineers in the materials and medical fields.[2] Currently, autologous bones and commercial artificial bones are the primary options for repair of load-bearing bone defects. Because of the disadvantages of autologous and commercially available artificial bones, as described in the Introduction above, significant interest in the development of new artificial bones has been expressed by the medical community. Ideally, artificial bones should have chemical and structural compositions similar to natural bones, and they should have shaping ability and biomechanics similar to natural bones. Additionally, artificial bones should also be

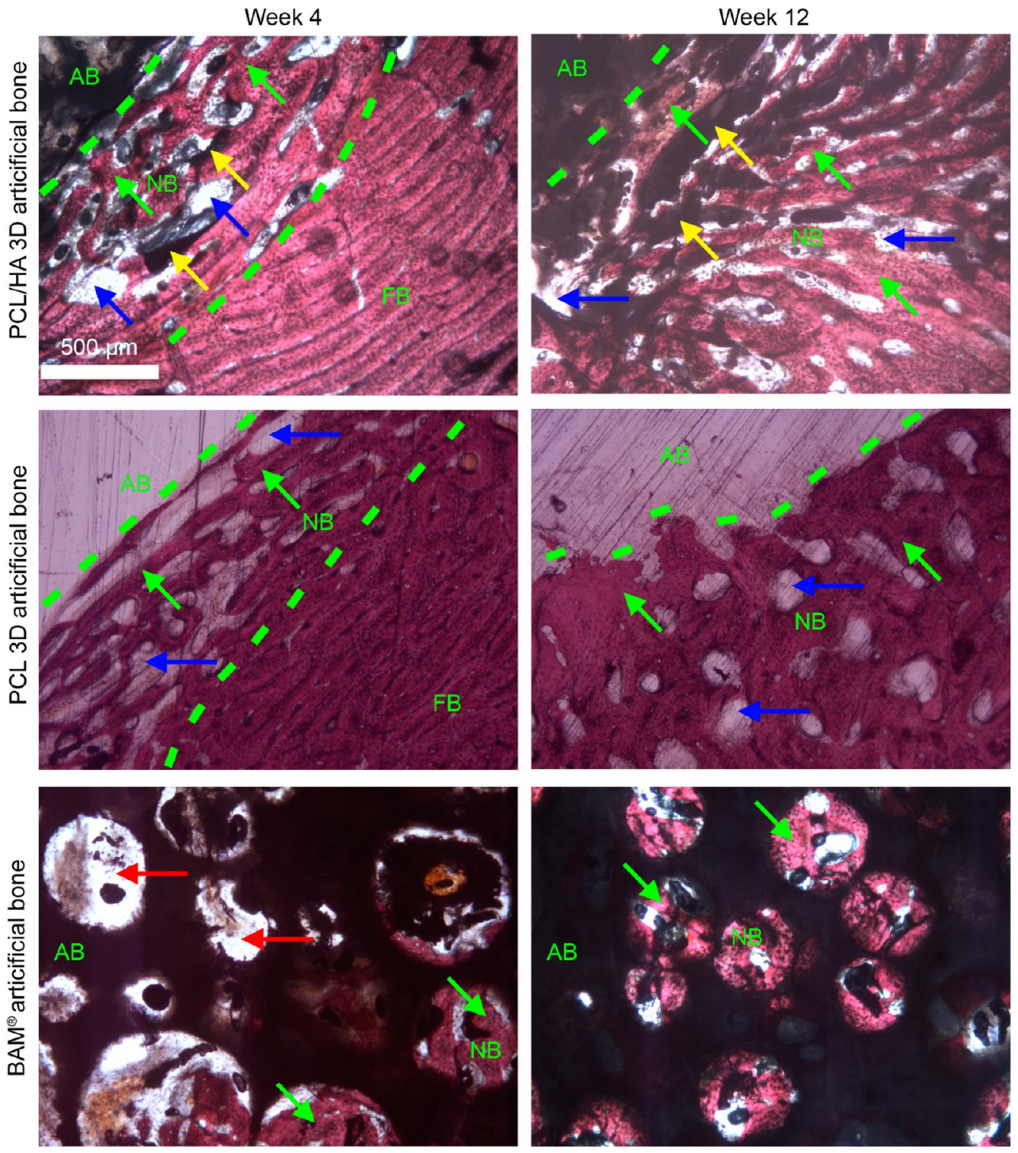

Figure 8. Histological observation of the interfaces between implanted materials and the surrounding bones at 4 and 12 weeks postimplantation by optical microscopy. AB, artificial bone; FB, natural goat femur bone; NB, new bone. Dashed lines indicate edges between AB and NB or between FB and NB. Green arrows indicate NB. Blue arrows indicate PCL pieces. Yellow arrows indicate HA pieces. Red arrows indicate the pores of BAM artificial bone. The scale bar is 500 μm and applies to all images.

biocompatibible and induce the appropriate formation of new bone. Artificial bones should also be biodegradable with a biodegradation rate that matches that of new bone formation. Finally, artificial bones should be easily produced by manufacturers, easily utilized by surgeons, and be benficial to patients.

In this work, PCL/HA and PCL 3D artificial bones (Figure 2) were fabricated by CT-guided FDM to mimic natural goat femurs. The 3D artificial bones had both cortical bonelike feature and cancellous bonelike features (porous scaffolds). Compared with organic PCL 3D artificial bone, the PCL/HA 3D artificial bone was an inorganic/organic composite.

Ideally, implantable artificial bones should be easily shaped and have similar biomechanics to the surrounding native bone, as these properties could decrease the risk of the bone refractures.[34] The in vitro compression measurements (Figure 3 and Table 1) demonstrated that the order of compressive strength and elastic modulus of the tested materials was as follows: adult goat femur > PCL/HA 3D artificial bone > PCL 3D artificial bone > BAM artificial bone. The porous structure of the BAM artificial bone may contribute to its relatively low biomechanical properties. The compression measurements confirmed that the biomechanical properties of PCL/HA 3D artificial bone are more similar to natural bone. Moreover, the artificial bones that were fabricated by CT-guided FDM had shapes that were more similar to natural bones (Figure 2) than the BAM artificial bone. Therefore, PCL/HA 3D artificial bones demonstrated better shaping ability and biomechanical properties in these studies.

Biocompatibility is also a significant factor in the development of medical implants.[35] Both PCL and HA have previously proven to be biocompatible.[36,37] In this work, the biocompatibility of PCL/HA and PCL 3D artificial bones was studied. The in vitro cell biocompatibility studies (Figure 4) showed that MC3T3-E1 cells proliferated well on the three artificial bone biomaterials, which indicated that the three biomaterials

possessed good biocompatibility. The relative in vitro cell proliferation ability of the three materials was as follows: BAM artificial bone > PCL/HA scaffold > PCL scaffold. The possible reasons for these trends include: (1) PCL degradation induces an acidic environments,[38,39] which may decrease cell proliferation on PCL scaffolds; and (2) HA is a weak alkaline calcium phosphates and can neutralize the acidity of PCL degradation products; therefore, HA has excellent cell biocompatibility.[40] The in vivo implantation studies (Figures 7 and 8) showed that the degradation products of the three artificial bones fused with new bones, indicating that the tested artificial bones had good in vivo biocompatibility. Therefore, this work suggested that PCL/HA and PCL 3D artificial bones had good in vitro and in vivo biocompatibility.

Appropriate new bone formation and matching of new bone formation rates with artificial bone biodegradation rates at the interface are important for the bone repair.[41] Both overformation of new bone and overbiodegradation of artificial bone could result in undesirable bone repair. It is well-known that normal bone fracture healing time is approximately 3 months. To evaluate the relationship between new bone formation and artificial bone biodegradation, we implanted the artificial bones in long load-bearing goat femur segmental bone defect model. X-ray images (Figure 6) at 12 weeks postimplantation showed that BAM artificial bones induced excess callus that could induce bone mal union, PCL 3D artificial bones induced slow new bone formation that could induce delayed bone union, and PCL/HA 3D artificial bones induced appropriate new bone formation at the interface between the artificial bone and the surrounding femur bone. Both PCL and HA are well-known biodegradable materials,[42,43] which ensures biodegradation of the 3D artificial bones. As shown in Figures 7 and 8, histological evaluation confirmed that PCL/HA and PCL 3D artificial bones could be degraded and could fuse with the surrounding new bone environment. Therefore, according to X-ray (Figure 6) and histological observations (Figures 7 and 8), PCL/HA 3D artificial bone induced appropriate artificial bone degradation and new bone formation at 3 months. Moreover, the biodegradation rate of the PCL/HA 3D artificial bones matched the formation rate of new bones.

The research and development of ideal artificial bones should also include consideration of easy production for manufacturers, easy operability for surgeons, and patient satisfaction. The fabrication of PCL/HA and PCL 3D artificial bones (Figure 2) showed CT-guided FDM is simple, effective, feasible, and convenient. Moreover, implanted 3D artificial bones could be easily cut from fabricated 3D artificial bones to match bone defect sizes. This method allows for facile fabrication of an entire 3D artificial bone and subsequent implantation of a desired portion. Using CT-guided FDM, PCL/HA and PCL 3D artificial bones could be easily fabricated by manufacturers and potentially used in hospitals. The segmental bone defect model construction and artificial bone implantation (Figure 5) was facile and quick (approximately 20 min). Thus, implantation of these new artificial bones for the treatment of load-bearing bone defects could be easily carried out by surgeons. Additionally, during the whole implantation process and the subsequent 3 months, the goats in this study did not show obvious discomfort, indicating that the PCL/HA and PCL 3D artificial bones could potentially promote high patient satisfaction.

During the past 30 years, various bioceramic, polymeric, and bioceramic/polymeric composite scaffolds have been investigated for the treatment of load-bearing segmental bone defects.[29,44] In particular, artificial porous bioceramics and bioceramic/polymeric composite scaffolds have attracted increasing attention due to their interconnected pores that have the potential to guide cell attachment and growth/ingrowth.[28] Compared with previously developed porous bioceramics[45,46] and bioceramic/polymeric composite scaffolds,[47−50] our 3D artificial bones consisted of a PCL/HA composite with both cancellous bonelike features (porous scaffold) and cortical bonelike features. PCL has previously demonstrated good mechanical properties and a reduced degradation rate compared with other polymers.[51−53] HA is the most commonly used bioceramic because of its biocompatibility[54] and slow degradation rate.[55]

PCL/HA scaffolds have been previously developed and characterized.[28,51,56−61] In particular, the in vivo behaviors of porous PCL/HA-cell scaffolds were investigated.[51,61] In these studies, cells such as osteoblasts[51] or chondrocytes and bone marrow stromal cells[61] were seeded onto porous PCL/HA scaffolds that were then implanted in the backs of Balb-C nude mice[51] or goat femoral heads,[61] respectively. These porous PCL/HA-cell scaffolds demonstrated increased tissue growth ability. In our work, PCL/HA 3D artificial bones without prior cell seeding showed appropriate biodegradation and bone regeneration ability. The porous side of the cut PCL/HA 3D artificial bones faced the femoral shaft. Therefore, in our work, the porous PCL/HA scaffold (cancellous bonelike feature) could play the primary role in bone regeneration by guiding cell attachment and growth/ingrowth.[28] The presence of the cortical bonelike feature in the PCL/HA scaffold may be the source of improved biomechanical property matching to natural bones. In contrast to previous studies,[51,61] our work also implied that preimplantation cell seeding may not be necessary for PCL/HA scaffolds to promote in vivo tissue repair.

5. CONCLUSIONS

In this work, CT-guided FDM was used to fabricate 3D artificial bones with both cortical bonelike and cancellous bonelike features. Then, the in vitro mechanical properties, the in vitro cell biocompatibility, and the in vivo behaviors of the scaffolds were investigated. Compared with BAM artificial bones and PCL 3D artificial bones, PCL/HA 3D artificial bones had several advantages: (i) good biomimetics to native bones in terms of both chemical composition and structure, as it is possible to fabricate PCL/HA 3D artificial bones that match the shape and biomechanical characteristics of bone defect sites; (ii) good shaping ability and biomechanics; (iii) good in vitro and in vivo biocompactibility; (iv) appropriate formation of new bone and matching between the artificial bone biodegradation and new bones formation rates; and (v) easy producibility for manufacturers, and easy operability for surgeons. Therefore, CT-guided FDM is simple, convenient, relatively low-cost and suitable for the fabrication of natural bonelike artificial bones. In addition, this work suggests that PCL/HA 3D artificial bones could potentially be used to treat load-bearing goat femur segmental bone defects and could benefit patients with bone repair needs. Previous work has demonstrated that scaffold pore sizes greatly influence cellular activity,[62] Therefore, further work is necessary to study the effects of the pore distribution and scaffold dimensions on bone regeneration. Further, the mechanical properties of repairing bones after implantation in in vivo studies should be also investigated.

AUTHOR INFORMATION

Corresponding Authors

*E-mail: xuguohuamail@163.com. Fax: +86-21-63520020.
*E-mail: jianzhongpku@hotmail.com. Fax: +86-21-34291125.

Author Contributions

†N.X. and X.Y. contributed equally to this work.

Notes

The authors declare no competing financial interest.

ACKNOWLEDGMENTS

This research has been supported by research grants from the National Natural Science Foundation of China (81271954, 81301537, 51203024), the Nanotechnology Program of Shanghai Science & Technology Committee, Shanghai (11 nm0504200), the National High Technology Research and Development Program of China (863 Program 2013AA032203, 2012AA030309), the Shanghai Pujiang Talent Program (12PJ1430300), the Special Fund for Talents in Minhang District of Shanghai (2012).

REFERENCES

(1) Dimitriou, R.; Jones, E.; McGonagle, D.; Giannoudis, P. Bone Regeneration: Current Concepts and Future Directions. *BMC Med.* **2011**, *9*, 66.

(2) Berner, A.; Reichert, J.; Müller, M.; Zellner, J.; Pfeifer, C.; Dienstknecht, T.; Nerlich, M.; Sommerville, S.; Dickinson, I.; Schütz, M.; Füchtmeier, B. Treatment of Long Bone Defects and Non-unions: from Research to Clinical Practice. *Cell Tissue Res.* **2012**, *347*, 501−519.

(3) Zeitouni, S.; Krause, U.; Clough, B. H.; Halderman, H.; Falster, A.; Blalock, D. T.; Chaput, C. D.; Sampson, H. W.; Gregory, C. A. Human Mesenchymal Stem Cell−Derived Matrices for Enhanced Osteoregeneration. *Sci. Transl. Med.* **2012**, *4*, 132ra55.

(4) Giannoudis, P. V.; Dinopoulos, H.; Tsiridis, E. Bone Substitutes: An Update. *Injury* **2005**, *36*, S20−S27.

(5) Pape, H. C.; Evans, A.; Kobbe, P. Autologous Bone Graft: Properties and Techniques. *J. Orthop. trauma* **2010**, *24*, S36−40.

(6) Marsh, D. Concepts of Fracture Union, Delayed Union, and Nonunion. *Clin. Orthop. Relat. Res.* **1998**, *355*, S22−S30.

(7) *United States Bone and Joint Decade: The Burden of Musculoskeletal Diseases and Musculoskeletal Injuries in the United States*; American Academy of Orthopedic Surgeons: Rosemont, IL, 2008; http://www.boneandjointburden.org/ (accessed August 14, 2014).

(8) Rho, J.-Y.; Kuhn-Spearing, L.; Zioupos, P. Mechanical Properties and the Hierarchical Structure of Bone. *Med. Eng. Phys.* **1998**, *20*, 92−102.

(9) Sopyan, I.; Mel, M.; Ramesh, S.; Khalid, K. A. Porous Hydroxyapatite for Artificial Bone Applications. *Sci. Technol. Adv. Mater.* **2007**, *8*, 116−123.

(10) Yuan, J.; Cui, L.; Zhang, W. J.; Liu, W.; Cao, Y. Repair of Canine Mandibular Bone Defects with Bone Marrow Stromal Cells and Porous β-tricalcium Phosphate. *Biomaterials* **2007**, *28*, 1005−1013.

(11) Kikuchi, M.; Itoh, S.; Ichinose, S.; Shinomiya, K.; Tanaka, J. Self-organization Mechanism in a Bone-like Hydroxyapatite/collagen Nanocomposite Synthesized In Vitro and its Biological Reaction In Vivo. *Biomaterials* **2001**, *22*, 1705−1711.

(12) Lei, Y.; Rai, B.; Ho, K. H.; Teoh, S. H. In Vitro Degradation of Novel Bioactive Polycaprolactone—20% Tricalcium Phosphate Composite Scaffolds for Bone Engineering. *Mater. Sci. Eng., C* **2007**, *27*, 293−298.

(13) Liu, H.; Peng, H.; Wu, Y.; Zhang, C.; Cai, Y.; Xu, G.; Li, Q.; Chen, X.; Ji, J.; Zhang, Y.; OuYang, H. W. The Promotion of Bone Regeneration by Nanofibrous Hydroxyapatite/chitosan Scaffolds by Effects on Integrin-BMP/Smad Signaling Pathway in BMSCs. *Biomaterials* **2013**, *34*, 4404−4417.

(14) Reichert, J. C.; Cipitria, A.; Epari, D. R.; Saifzadeh, S.; Krishnakanth, P.; Berner, A.; Woodruff, M. A.; Schell, H.; Mehta, M.; Schuetz, M. A.; Duda, G. N.; Hutmacher, D. W. A Tissue Engineering Solution for Segmental Defect Regeneration in Load-Bearing Long Bones. *Sci. Transl. Med.* **2012**, *4*, 141ra93.

(15) Kumar, S.; Kruth, J. P. Composites by Rapid Prototyping Technology. *Mater. Des.* **2010**, *31*, 850−856.

(16) Lantada, A. D.; Morgado, P. L. Rapid Prototyping for Biomedical Engineering: Current Capabilities and Challenges. *Annu. Rev. Biomed. Eng.* **2012**, *14*, 73−96.

(17) Zein, I.; Hutmacher, D. W.; Tan, K. C.; Teoh, S. H. Fused Deposition Modeling of Novel Scaffold Architectures for Tissue Engineering Applications. *Biomaterials* **2002**, *23*, 1169−1185.

(18) Hutmacher, D. W.; Schantz, T.; Zein, I.; Ng, K. W.; Teoh, S. H.; Tan, K. C. Mechanical Properties and Cell Cultural Response of Polycaprolactone Scaffolds Designed and Fabricated via Fused Deposition Modeling. *J. Biomed. Mater. Res.* **2001**, *55*, 203−216.

(19) Meakin, J. R.; Shepherd, D. E. T.; Hukins, D. W. L. Fused Deposition Models from CT Scans. *Br. J. Radiol.* **2004**, *77*, 504−507.

(20) Tuan, H. S.; Hutmacher, D. W. Application of Micro CT and Computation Modeling in Bone Tissue Engineering. *Comput. Aided Des.* **2005**, *37*, 1151−1161.

(21) Zeng, W.; Lin, F.; Shi, T.; Zhang, R.; Nian, Y.; Ruan, J.; Zhou, T. Fused Deposition Modelling of an Auricle Framework for Microtia Reconstruction based on CT Images. *Rapid Prototyping J.* **2008**, *14*, 280−284.

(22) Tellis, B. C.; Szivek, J. A.; Bliss, C. L.; Margolis, D. S.; Vaidyanathan, R. K.; Calvert, P. Trabecular Scaffolds Created using Micro CT Guided Fused Deposition Modeling. *Mater. Sci. Eng., C* **2008**, *28*, 171−178.

(23) Fan, C.; Li, J.; Xu, G.; He, H.; Ye, X.; Chen, Y.; Sheng, X.; Fu, J.; He, D. Facile Fabrication of Nano-hydroxyapatite/silk Fibroin Composite via a Simplified Coprecipitation Route. *J. Mater. Sci.* **2010**, *45*, 5814−5819.

(24) Sun, G.; Wei, D.; Liu, X.; Chen, Y.; Li, M.; He, D.; Zhong, J. Novel Biodegradable Electrospun Nanofibrous P(DLLA-CL) Balloons for the Treatment of Vertebral Compression Fractures. *Nanomedicine (N. Y., NY, U. S.)* **2013**, *9*, 829−838.

(25) Lucas-Girot, A.; Langlois, P.; Sangleboeuf, J. C.; Ouammou, A.; Rouxel, T.; Gaude, J. A Synthetic Aragonite-based Bioceramic: Influence of Process Parameters on Porosity and Compressive Strength. *Biomaterials* **2002**, *23*, 503−510.

(26) Gomes, F. O.; Pires, R. A.; Reis, R. L. Aluminum-free Glass-ionomer Bone Cements with Enhanced Bioactivity and Biodegradability. *Mater. Sci. Eng., C* **2013**, *33*, 1361−1370.

(27) Cheng, S.-T.; Chen, Z.-F.; Chen, G.-Q. The Expression of Cross-linked Elastin by Rabbit Blood Vessel Smooth Muscle Cells Cultured in Polyhydroxyalkanoate Scaffolds. *Biomaterials* **2008**, *29*, 4187−4194.

(28) Park, S.; Lee, S.; Kim, W. Fabrication of Porous Polycaprolactone/Hydroxyapatite (PCL/HA) Blend Scaffolds using a 3D Plotting System for Bone Tissue Engineering. *Bioprocess Biosyst. Eng.* **2011**, *34*, 505−513.

(29) Pilia, M.; Guda, T.; Appleford, M. Development of Composite Scaffolds for Load-Bearing Segmental Bone Defects. *BioMed. Res. Int.* **2013**, *2013*, 15.

(30) Eshraghi, S.; Das, S. Mechanical and Microstructural Properties of Polycaprolactone Scaffolds with One-Dimensional, Two-Dimensional, and Three-Dimensional Orthogonally Oriented Porous Architectures Produced by Selective Laser Sintering. *Acta Biomater.* **2010**, *6*, 2467−2476.

(31) Nejati, E.; Mirzadeh, H.; Zandi, M. Synthesis and Characterization of Nano-hydroxyapatite Rods/Poly(l-lactide acid) Composite Scaffolds for Bone Tissue Engineering. *Composites, Part A* **2008**, *39*, 1589−1596.

(32) Sun, H.; Mei, L.; Song, C.; Cui, X.; Wang, P. The In Vivo Degradation, Absorption and Excretion of PCL-Based Implant. *Biomaterials* **2006**, *27*, 1735−1740.

(33) *Implantable Medical Devices: US Industry Forecasts for 2014 & 2019*; The Freedonia Group: Cleveland, OH, 2010; http://www.freedoniagroup.com/brochure/25xx/2595embro.pdf (accessed August 14, 2014).
(34) Wähnert, D.; Hoffmeier, K. L.; Klos, K.; Stolarczyk, Y.; Fröber, R.; Hofmann, G. O.; Mückley, T. Biomechanical Characterization of an Osteoporotic Artificial Bone Model for the Distal Femur. *J. Biomater. Appl.* **2012**, *26*, 565−579.
(35) Williams, D. F. On the Mechanisms of Biocompatibility. *Biomaterials* **2008**, *29*, 2941−2953.
(36) Sinha, V. R.; Bansal, K.; Kaushik, R.; Kumria, R.; Trehan, A. Poly-ε-Caprolactone Microspheres and Nanospheres: an Overview. *Int. J. Pharm.* **2004**, *278*, 1−23.
(37) Tsiridis, E.; Bhalla, A.; Ali, Z.; Gurav, N.; Heliotis, M.; Deb, S.; DiSilvio, L. Enhancing the Osteoinductive Properties of Hydroxyapatite by the Addition of Human Mesenchymal Stem Cells, and Recombinant Human Osteogenic Protein-1 (BMP-7) In Vitro. *Injury* **2006**, *37*, S25−S32.
(38) Williams, D. F. Mechanisms of Biodegradation of Implantable Polymers. *Clin. Mater.* **1992**, *10*, 9−12.
(39) Coombes, A. G. A.; Meikle, M. C. Resorbable Synthetic Polymers as Replacements for Bone Graft. *Clin. Mater.* **1994**, *17*, 35−67.
(40) Zhang, D.; Zhao, H.; Zhao, X.; Liu, Y.; Chen, H.; Li, X. Application of Hydroxyapatite as Catalyst and Catalyst Carrier. *Huaxue Jinzhan* **2011**, *23*, 687−694.
(41) Arinzeh, T. L.; Tran, T.; McAlary, J.; Daculsi, G. A Comparative Study of Biphasic Calcium Phosphate Ceramics for Human Mesenchymal Stem-Cell-Induced Bone Formation. *Biomaterials* **2005**, *26*, 3631−3638.
(42) Messersmith, P. B.; Giannelis, E. P. Synthesis and Barrier Properties of Poly(ε-caprolactone)-Layered Silicate Nanocomposites. *J. Polym. Sci., Part A: Polym. Chem.* **1995**, *33*, 1047−1057.
(43) Hench, L. L. Bioceramics. *J. Am. Ceram. Soc.* **1998**, *81*, 1705−1728.
(44) Ding, S.-J.; Shie, M.-Y.; Wei, C.-K. In Vitro Physicochemical Properties, Osteogenic Activity, and Immunocompatibility of Calcium Silicate−Gelatin Bone Grafts for Load-Bearing Applications. *ACS Appl. Mater. Interfaces* **2011**, *3*, 4142−4153.
(45) Baino, F.; Verné, E.; Vitale-Brovarone, C. 3-D High-strength Glass−ceramic Scaffolds Containing Fluoroapatite for Load-bearing Bone Portions Replacement. *Mater. Sci. Eng., C* **2009**, *29*, 2055−2062.
(46) Ramay, H. R. R.; Zhang, M. Biphasic Calcium Phosphate Nanocomposite Porous Scaffolds for Load-bearing Bone Tissue Engineering. *Biomaterials* **2004**, *25*, 5171−5180.
(47) Wang, H.; Li, Y.; Zuo, Y.; Li, J.; Ma, S.; Cheng, L. Biocompatibility and Osteogenesis of Biomimetic Nano-hydroxyapatite/Polyamide Composite Scaffolds for Bone Tissue Engineering. *Biomaterials* **2007**, *28*, 3338−3348.
(48) Cao, H.; Kuboyama, N. A Biodegradable Porous Composite Scaffold of PGA/β-TCP for Bone Tissue Engineering. *Bone* **2010**, *46*, 386−395.
(49) Chu, T.-M. G.; Warden, S. J.; Turner, C. H.; Stewart, R. L. Segmental Bone Regeneration using a Load-bearing Biodegradable Carrier of Bone Morphogenetic Protein-2. *Biomaterials* **2007**, *28*, 459−467.
(50) Rai, B.; Lin, J. L.; Lim, Z. X. H.; Guldberg, R. E.; Hutmacher, D. W.; Cool, S. M. Differences between In Vitro Viability and Differentiation and In Vivo Bone-forming Efficacy of Human Mesenchymal Stem Cells Cultured on PCL−TCP Scaffolds. *Biomaterials* **2010**, *31*, 7960−7970.
(51) Chim, H.; Hutmacher, D. W.; Chou, A. M.; Oliveira, A. L.; Reis, R. L.; Lim, T. C.; Schantz, J. T. A Comparative Analysis of Scaffold Material Modifications for Load-bearing Applications in Bone Tissue Engineering. *Int. J. Oral Maxillofac. Surg.* **2006**, *35*, 928−934.
(52) Roohani-Esfahani, S.-I.; Nouri-Khorasani, S.; Lu, Z.; Appleyard, R.; Zreiqat, H. The Influence Hydroxyapatite Nanoparticle Shape and Size on the Properties of Biphasic Calcium Phosphate Scaffolds Coated with Hydroxyapatite−PCL Composites. *Biomaterials* **2010**, *31*, 5498−5509.
(53) Fabbri, P.; Cannillo, V.; Sola, A.; Dorigato, A.; Chiellini, F. Highly Porous Polycaprolactone-45S5 Bioglass® Scaffolds for Bone Tissue Engineering. *Compos. Sci. Technol.* **2010**, *70*, 1869−1878.
(54) Wei, G.; Ma, P. X. Structure and Properties of Nano-hydroxyapatite/Polymer Composite Scaffolds for Bone Tissue Engineering. *Biomaterials* **2004**, *25*, 4749−4757.
(55) Polini, A.; Pisignano, D.; Parodi, M.; Quarto, R.; Scaglione, S. Osteoinduction of Human Mesenchymal Stem Cells by Bioactive Composite Scaffolds without Supplemental Osteogenic Growth Factors. *PLoS One* **2011**, *6*, e26211.
(56) Yu, H.; Wooley, P.; Yang, S.-Y. Biocompatibility of Poly-epsilon-caprolactone-hydroxyapatite Composite on Mouse Bone Marrow-derived Osteoblasts and Endothelial Cells. *J. Orthop. Surg. Res.* **2009**, *4*, 5.
(57) Koh, Y.-H.; Jun, I.-K.; Kim, H.-E. Fabrication of Poly(ε-caprolactone)/hydroxyapatite Scaffold using Rapid Direct Deposition. *Mater. Lett.* **2006**, *60*, 1184−1187.
(58) Bawolin, N. K.; Li, M. G.; Chen, X. B.; Zhang, W. J. Modeling Material-Degradation-Induced Elastic Property of Tissue Engineering Scaffolds. *J. Biomech. Eng.* **2010**, *132*, 111001−111001.
(59) Shor, L.; Güçeri, S.; Wen, X.; Gandhi, M.; Sun, W. Fabrication of Three-dimensional Polycaprolactone/hydroxyapatite Tissue Scaffolds and Osteoblast-scaffold Interactions In Vitro. *Biomaterials* **2007**, *28*, 5291−5297.
(60) Yeong, W. Y.; Sudarmadji, N.; Yu, H. Y.; Chua, C. K.; Leong, K. F.; Venkatraman, S. S.; Boey, Y. C. F.; Tan, L. P. Porous Polycaprolactone Scaffold for Cardiac Tissue Engineering Fabricated by Selective Laser Sintering. *Acta Biomater.* **2010**, *6*, 2028−2034.
(61) Ding, C.; Qiao, Z.; Jiang, W.; Li, H.; Wei, J.; Zhou, G.; Dai, K. Regeneration of a Goat Femoral Head using a Tissue-specific, Biphasic Scaffold Fabricated with CAD/CAM Technology. *Biomaterials* **2013**, *34*, 6706−6716.
(62) Murphy, C. M.; Haugh, M. G.; O'Brien, F. J. The Effect of Mean Pore Size on Cell Attachment, Proliferation and Migration in Collagen−glycosaminoglycan Scaffolds for Bone Tissue Engineering. *Biomaterials* **2010**, *31*, 461−466.
(63) Yaszemski, M. J.; Payne, R. G.; Hayes, W. C.; Langer, R.; Mikos, A. C. Evolution of Bone Transplantation: Molecular, Cellular, and Tissue Strategies to Engineer Human Bone. *Biomaterials* **1996**, *17*, 175−185.
(64) Gerhart, T. N.; Renshaw, A. A.; Miller, R. L.; Noecker, R. J.; Hayes, W. C. In Vivo Histologic and Biomechanical Characterization of a Biodegradable Particulate Composite Bone Cement. *J. Biomed. Mater. Res.* **1989**, *23*, 1−16.